# Dysregulation of extracellular fibronectin and α5-integrin in dermal aging

Yaelim Lee[a], Xingyu Shen[a], Oliver Dreesen[a,b], Jin Zhu[a], and Rong Li[a,c,*]
[a]Mechanobiology Institute, National University of Singapore, Singapore 117411; [b]A*STAR Skin Research Labs (A*SRL), Agency for Science, Technology and Research (A*STAR), Singapore 138648 ; [c]Department of Biological Sciences, National University of Singapore, Singapore 117558

**ABSTRACT** **Dermal aging is a complex process characterized by structural and functional changes in the extracellular matrix (ECM) and the resident cells, such as dermal fibroblasts. Fibronectin (FN) ECM is a crucial component of the dermis, yet its role in natural aging remains poorly understood. Here, we demonstrate a significant reduction in FN ECM in aged, otherwise healthy, mouse dermis. To explore whether aging dermal fibroblasts contribute to this decline in FN levels, we examined human dermal fibroblasts (HDF) from aged skin and observed that they produce lower extracellular FN densities in vitro than young HDFs. This age-associated deficiency correlates with reduced level of α5-integrin, a cell-surface FN receptor essential for extracellular FN assembly. Knockdown of α5-integrin (α5KD) in young HDFs impairs FN ECM formation and induces phenotypes characteristic of cellular senescence. Interestingly, the proliferation defect in α5KD fibroblasts is largely restored by cell-derived matrices (CDMs) in vitro, highlighting the importance of ECM organization. These findings underscore the essential role of α5-integrin in maintaining proper ECM formation, which in turn protects against fibroblast senescence during dermal aging.**

## SIGNIFICANCE STATEMENT

- FN and α5-integrin are crucial for dermal ECM assembly, yet their roles in natural aging remain unclear. We show that aging diminishes FN ECM in mouse dermis and in aged HDFs, where α5-integrin is reduced.
- Knocking down α5-integrin in young fibroblasts induces senescence-like phenotypes and a transcriptional program characteristic of cellular senescence. Culturing α5-integrin–deficient and aged fibroblasts on CDMs restores their proliferation, underscoring the importance of integrin–ECM interactions in dermal aging.
- These findings elucidate how α5-integrin–FN interactions preserve dermal integrity, offering new insights for antiaging strategies targeting ECM organization and fibroblast function.

**Monitoring Editor**
Valerie Marie Weaver
University of California, San Francisco

Received: Feb 28, 2025
Revised: Jun 2, 2025
Accepted: Jun 16, 2025

This article was published online ahead of print in MBoC in Press (http://www.molbiolcell.org/cgi/doi/10.1091/mbc.E25-02-0074) on June 25 2025.

Author contributions: Y.L. and R.L. led all aspects of the study, including conceptualization, experimentation, data analysis, and manuscript writing; O.D. provided insights during discussions of the study's findings and contributed to manuscript review and revisions; X.Y. and J.Z. assisted in experimental analysis. All authors reviewed and approved the final manuscript.

Conflicts of interest: The authors declare no financial conflict of interest.

*Address correspondence to: Rong Li (mbihead@nus.edu.sg).

Abbreviations used: ECM, extracellular matrix; FN, fibronectin; HDFs, human dermal fibroblasts; MMP, matrix metalloproteinase; aHDFs, aged human

## INTRODUCTION

As humans age, the dermis undergoes significant structural and compositional changes in the extracellular matrix (ECM), accompanied by functional decline in resident fibroblasts. Fibroblasts, the primary cells responsible for ECM production and remodeling, play a crucial role in maintaining dermal integrity (Plikus *et al.*, 2021). However, age-related alterations in the dermal microenvironment disrupt cellular communication and impair fibroblast function, contributing to various skin disorders such as chronic wounds, increased susceptibility to infections, inflammation, and a higher incidence of skin cancers (Haydont *et al.*, 2019; Fane and Weeraratna, 2020).

One of the best known age-related changes in ECM is the decline in collagen density and organization. Collagen fibrils, particularly types I and III, which provide structural integrity to the dermis, become fragmented due to increased matrix metalloproteinase activity and reduced collagen synthesis (Fligiel *et al.*, 2003; Varani *et al.*, 2006; Fisher *et al.*, 2009; Panwar *et al.*, 2018; Haydont *et al.*, 2019; McCabe *et al.*, 2020). The loss of collagen's dense, basket-weave structure, along with the accumulation of fragmented fibrils, results in a less cohesive matrix with larger gaps between fibers (Fane and Weeraratna, 2020). This structural degradation manifests as visible signs of aging, such as wrinkles, thinning skin, and reduced elasticity (Haydont *et al.*, 2019).

Accompanying such ECM changes, dermal fibroblasts undergo significant functional decline and a reduction in number with aging (Varani *et al.*, 2006; Sole-Boldo *et al.*, 2020). The remaining fibroblasts in the aged dermis often acquire a senescent phenotype, characterized by cell-cycle arrest and secretion of pro-inflammatory factors (senescence-associated secretory phenotype) (Chin *et al.*, 2023). Moreover, fibroblasts from aged skin exhibit a reduced ability to remodel the ECM (Cole *et al.*, 2018), loss of distinct identities typically maintained in the young dermis, and weakened interactions with other skin cells (Sole-Boldo *et al.*, 2020).

The origin of the above age-associated changes remain poorly understood. Fibronectin (FN) is the first ECM protein incorporated into the remodeling ECM (Singh *et al.*, 2010) and plays a pivotal role in the initial stages of ECM formation, serving as a scaffold for other ECM proteins, including collagens (McDonald *et al.*, 1982; Sottile *et al.*, 2007; Singh *et al.*, 2010; Graham *et al.*, 2019).

$\alpha$5:$\beta$1-integrin is a heterodimeric FN receptor present on the fibroblast plasma membrane, and its interaction with FN is required for extracellular FN fibril formation (Singh *et al.*, 2010; Schwarzbauer and DeSimone, 2011). Although extensive research has focused on age-associated changes in collagen ECM and fibroblasts, how FN ECM and its receptor, $\alpha$5-integrin, are altered during dermal aging—and how these changes affect fibroblast function and ECM integrity—remains largely unclear.

In this study, we investigated FN ECM in young and aged mouse to assess age-related changes in FN ECM. We further quantitatively compared the extracellular FN fibrils produced by aged human dermal fibroblasts (aHDF) and young HDFs (yHDF) to determine how aging affects extracellular FN fibrils formation. Additionally, we examined the role of $\alpha$5-integrin in the age-associated changes in FN ECM integrity and fibroblast function. By combining in vivo analysis of dermal tissues and in vitro experiments using primary HDFs, we provide evidence that age-associated changes in FN ECM and $\alpha$5-integrin contribute to fibroblast aging and dermal tissue homeostasis.

## RESULTS

### Age-related decline in dermal FN ECM in vivo and in vitro

To assess age-related changes in FN ECM, we analyzed skin tissue from young (1.5–3 mo) and aged (17–21 mo) mice, which correspond to humans under 20 y and over 55 y, respectively. Immunostaining for FN in mouse skin sections, followed by high-resolution confocal imaging, revealed a significant decrease in dermal FN levels in aged mice compared with young mice, with an average decrease of ~50% (Figure 1, A–C; Supplemental Figure S1).

To investigate the underlying cause of the age-associated reduction in FN levels, we hypothesized that aging of dermal fibroblasts—the primary cell type responsible for producing ECM proteins—contributes to this reduction. To test this, we cultured HDFs derived from young (10–11-y-old) and aged (70–80-y-old) skin biopsies (MATERIALS AND METHODS). Equal numbers of yHDFs and aHDFs were embedded in collagen-I gels within a three-dimensional (3D) culture system for 12 to 15 d, allowing sufficient time for the cells to deposit FN into the collagen-I ECM. In this 3D culture model, yHDFs proliferated significantly more and produced a denser FN network than aHDFs (Supplemental Figure S2A). However, we could not determine whether aHDFs had a reduced ability to produce extracellular FN due to the apparent proliferation defect of aHDF in this culture system.

To address this limitation, we further cultured yHDFs and aHDFs under comparable subconfluent conditions (~80% confluence) on standard tissue culture plates without any preexisting ECM. After 5 d of culture, proliferation differences between aHDFs and yHDFs were marginal, enabling a direct comparison of extracellular FN deposition. Immunofluorescence analysis of extracellular FN staining revealed that aHDFs produced discontinuous and short FN fibrils, whereas yHDFs generated continuous, interconnected fibrils forming a mesh-like structure (top panel, Figure 2A). To quantify this difference, we measured the mean volume of FN fibrils across multiple regions per sample using high-resolution confocal imaging. Despite being cultured under identical conditions with comparable surface occupancy (Supplemental Figure S2B), aHDFs exhibited a significant reduction in mean FN volume compared with yHDFs (Figure 2B). These findings underscore the age-related decline in fibroblasts' ability to produce and organize the FN ECM.

### $\alpha$5-integrin is reduced in aHDFs

To investigate the underlying basis of reduced FN density in aHDFs, we examined $\alpha$5-integrin levels. $\alpha$5-integrin is a crucial cell-surface receptor for FN and is highly expressed in HDFs (Supplemental Figure S3) and essential for the assembly of the extracellular FN matrix (Singh *et al.*, 2010). We performed immunofluorescent staining using the SNAKA51 antibody, which specifically recognizes the active form of $\alpha$5-integrin, in both young and aged HDFs. Our results showed that the cell-surface level of $\alpha$5-integrin was significantly reduced in aHDFs compared with yHDFs (Figure 3, A

dermal fibroblasts; yHDFs, young human dermal fibroblasts; 3D, three-dimensional; $\alpha$5KD, $\alpha$5-integrin knockdown; SA-$\beta$-gal, senescence-associated beta-galactosidase; RNA-seq, RNA-sequencing; DEGs, differentially expressed genes; GO, gene ontology; CDM, cell-derived matrix; GSEA, gene set enrichment analysis.

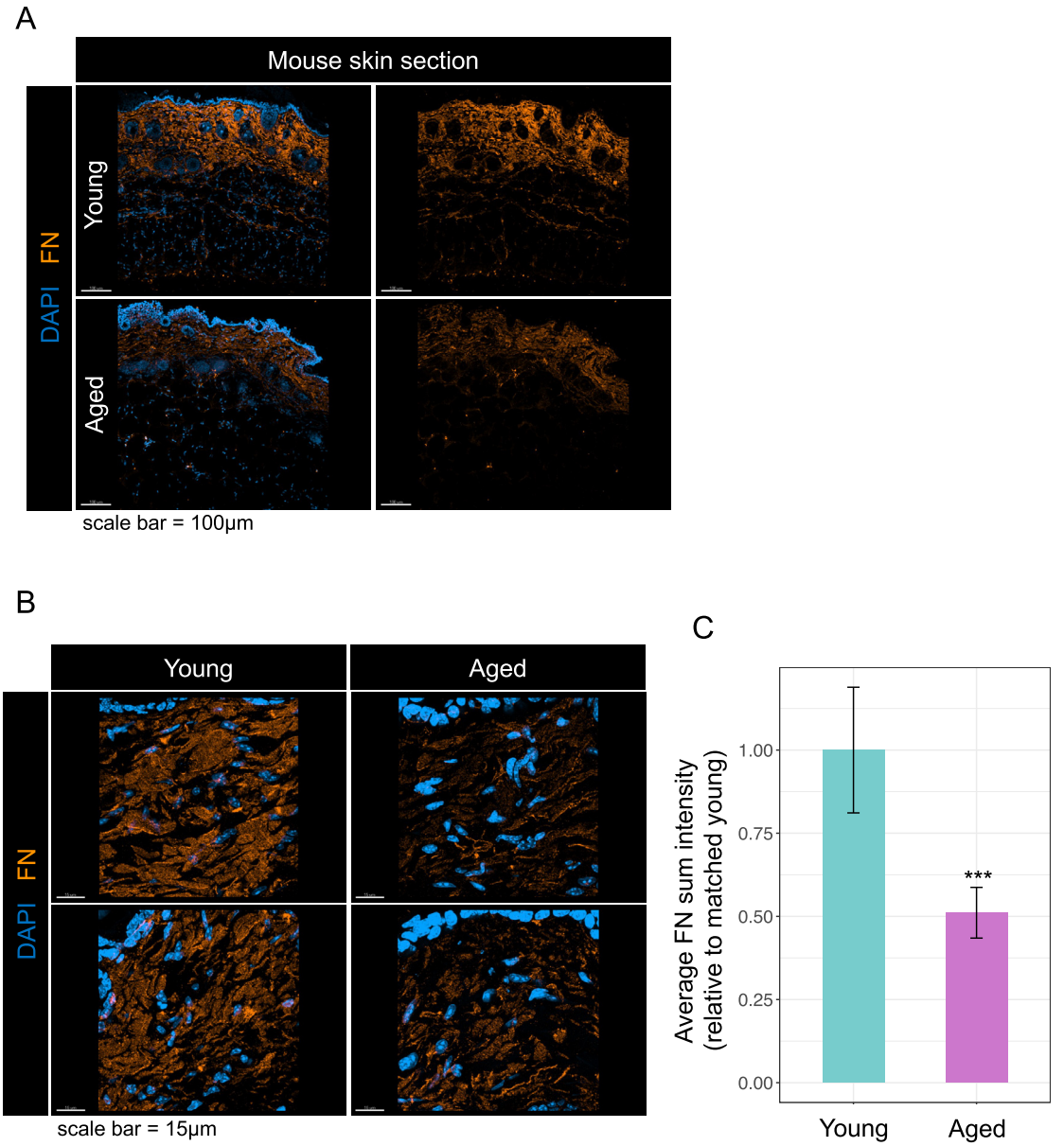


**FIGURE 1:** Extracellular FN ECM alterations in aged mouse dermis. (A) Representative immunofluorescence images of skin sections from young (top row) and aged (bottom row) mice, stained for FN (orange) and nuclei (DAPI, blue). (B) Representative high-magnification confocal images of the dermal FN in skin sections from young (left) and aged (right) mice. FN is shown in orange, and nuclei are stained with DAPI (blue). (C) Quantification of dermal FN signal intensity in skin sections from young and aged mice. Skin sections from three mice per group were analyzed, and multiple confocal images were acquired for each sample (see Supplemental Figure S1). Bars represent the average FN sum intensity, normalized to the matched young group, with error bars showing 95% confidence intervals. Statistical significance is indicated by ***$p < 0.001$ ($p = 6.95e{-}05$, Welch's *t* test).

and B). Western blot analysis confirmed that α5-integrin protein levels were significantly decreased by an average of 40 to 50% in aHDFs (Figure 3, C and D). It is noteworthy that the RNA expression level of α5-integrin (ITGA5) was unchanged in aHDF compared with yHDF lines that we utilized (Figure 3E), consistent with data from HDFs across a broader range of ages (Fleischer *et al.*, 2018) (Supplemental Figure S3). These findings suggest that the age-associated reduction in α5-integrin expression occurs via posttranscriptional mechanisms rather than transcriptional downregulation.

### Loss of α5-integrin recapitulates features of cellular senescence

In addition to reduced α5-integrin levels, aHDF showed a significant decrease in lamin-B1 levels (Figure 3, C and D), a key structural component of the nuclear lamina, whose reduction is a well-established marker of cellular senescence (Shimi *et al.*, 2011; Freund *et al.*, 2012; Dreesen *et al.*, 2013). We also examined PCNA, a widely used cell proliferation marker, and found that its levels were also significantly decreased in aHDFs, further supporting a senescent phenotype.

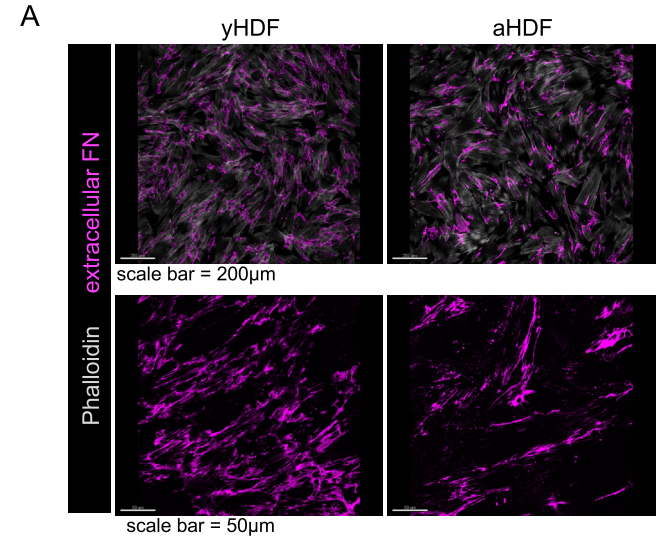


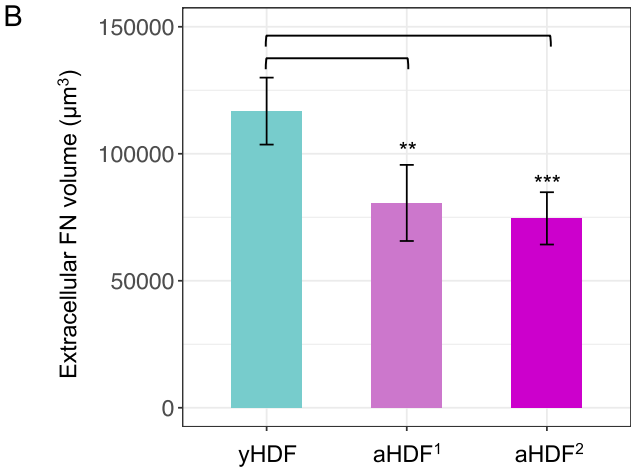


**FIGURE 2:** Reduced extracellular FN density in aHDFs. (A) Representative immunofluorescence images showing extracellular FN (magenta) and F-actin (phalloidin, gray) in yHDFs and aHDFs at low-magnification (top row) and high magnifications (bottom row). (B) Quantification of extracellular FN deposition, shown as the mean FN volume with 95% confidence intervals. Data are based on eight randomly selected positions per condition, comparing two aHDF lines derived from different aged donors (aHDF$^1$ and aHDF$^2$) with control yHDFs. Statistical significance is indicated by ***$p < 0.001$ and **$p < 0.01$ ($p = 3.27e{-}03$ for yHDF vs. aHDF$^1$; $p = 2.53e{-}04$ for yHDF vs. aHDF$^2$, Welch's *t* test).

Given the above finding, we next investigated whether there is a causal relationship between the loss of $\alpha$5-integrin and cellular senescence. To test this, we utilized siRNA-mediated knockdown (KD) of the gene encoding $\alpha$5-integrin (ITGA5) in young HDFs (yHDF) (Figure 4A). Following $\alpha$5-integrin KD ($\alpha$5KD), yHDFs exhibited noticeable morphological changes, shifting from their spindle-like shape to an enlarged and flattened appearance with prominent actin stress fibers (Figure 4B), reminiscent of features observed in senescent cells (Cho *et al.*, 2004). Notably, this $\alpha$5KD-induced morphological change parallels the difference seen between yHDFs and aHDFs (Supplemental Figure S4).

To determine whether $\alpha$5KD yHDFs exhibit cellular senescence, we performed senescence-associated beta-galactosidase (SA-$\beta$-gal) staining, a widely recognized marker of cellular senescence. We observed a significantly elevated SA-$\beta$-gal signal in $\alpha$5KD cells (Figure 4, C and D). In addition, lamin-B1 levels were markedly reduced in $\alpha$5KD fibroblasts (Figure 4, E and F), further supporting a senescence phenotype. Because cellular senescence is characterized by a permanent cell-cycle arrest, we also examined key proliferation markers, PCNA and Ki-67. Both markers were significantly decreased in $\alpha$5KD fibroblasts (Figure 4, E–H), suggesting a marked decline in proliferative capacity.

To further investigate the gene expression changes associated with $\alpha$5-integrin depletion, we performed RNA-sequencing (RNA-seq) analysis on $\alpha$5KD and control yHDFs. Differential gene expression analysis confirmed efficient ITGA5 KD and identified 246 significantly dysregulated genes (DEG, differentially expressed genes) by applying thresholds of fold-change and statistical significance (MATERIALS AND METHODS, Figure 5A). Gene ontology (GO) analysis of the downregulated DEGs highlighted key biological processes related to the mitotic cell cycle, particularly chromosome segregation, DNA replication, and microtubule cytoskeleton organization involved in mitotic spindle and kinetochore functions (Figure 5B; Supplemental Figure S5, top). A complete list of DEGs is provided in the Supplemental Information. These findings align with the senescence phenotype observed in $\alpha$5KD cells, which is characterized by loss of proliferative capacity.

Additionally, gene set enrichment analysis (GSEA) (Subramanian *et al.*, 2005) against established senescence-related gene sets (Tang *et al.*, 2007; Fridman and Tainsky, 2008; Saul *et al.*, 2022; Database, Reactome Pathway, 2024) revealed significant enrichment across all tested gene sets (Supplemental Figure S5, bottom). The most significantly enriched gene set was one downregulated in senescent primary fibroblasts following TP53 (p53 gene) inactivation (Tang *et al.*, 2007) (Figure 5C; Supplemental Figure S5, bottom). This result suggests that $\alpha$5KD induces a transcriptional program characteristics of cellular senescence.

Our RNA-seq analysis of $\alpha$5KD cells also identified 113 significantly upregulated DEGs (Figure 5A). GSEA based on expression changes across all genes indicated notable enrichment in several neuron-related GO terms. These terms included processes such as vesicle-mediated transport in synapses, neuron projection, axonogenesis, neuron migration, dendrite development, and synapse formation (Supplemental Figure S5, top). Lists of genes contributing to the highly enriched GO terms are listed in Supplemental Information. The biological significance of these neuronal signatures remains to be further explored.

### Cell-derived matrix rescues proliferation defects of $\alpha$5KD and aged fibroblasts

Next, we investigated how $\alpha$5-integrin loss could impede the proliferative potential in yHDFs. $\alpha$5-integrin, in conjunction with $\beta$1-integrin, forms a heterodimeric complex ($\alpha$5:$\beta$1-integrin) that binds to extracellular FN (Moreno-Layseca *et al.*, 2019). This interaction initiates intracellular signaling cascades that give rise to diverse downstream effects, often converging on regulation of the cell cycle. These signaling events ultimately influence whether the cells will continue to proliferate or exit the cell cycle (Giancotti and Ruoslahti, 1999; Hynes, 2002; Moreno-Layseca and Streuli, 2014).

$\alpha$5-integrin is also essential for forming FN ECM and subsequently collagen-I ECM (McDonald et al., 1982; Sottile *et al.*, 2007; Singh et al., 2010; Graham et al., 2019), which we confirmed in $\alpha$5KD fibroblasts (Figure 6A).

To determine whether ECM disruption, as opposed to signaling downstream of $\alpha$5-integrin, due to $\alpha$5-integrin loss contributes

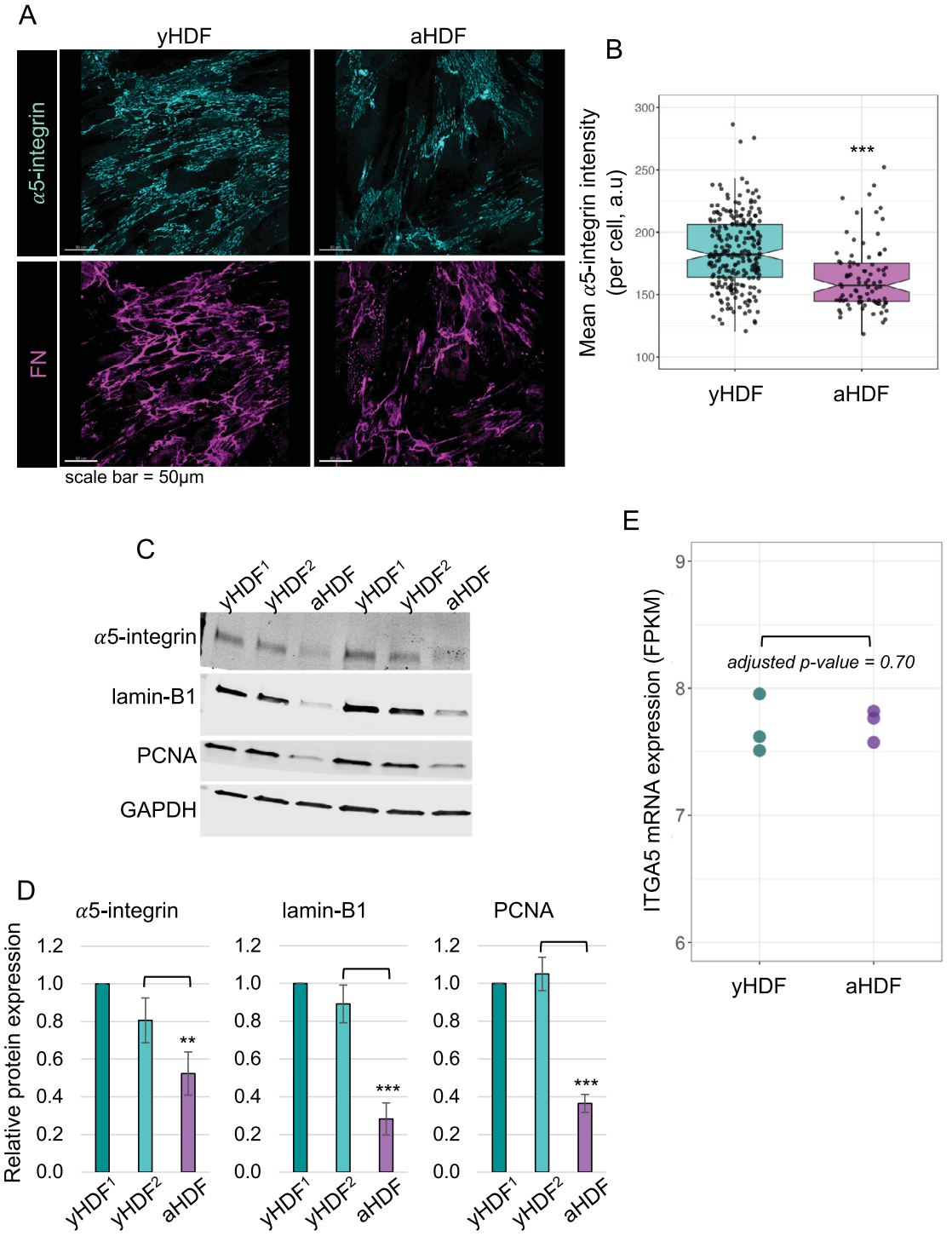


FIGURE 3: α5-integrin reduction in aHDFs. (A) Representative immunofluorescence images showing α5-integrin (cyan) and FN (magenta) in yHDFs and aHDFs. (B) Quantification of mean α5-integrin intensity per cell in yHDFs and aHDFs. ***$p < 0.001$ based on $n = 232$ for yHDFs and $n = 86$ for aHDFs ($p = 6.70e{-}09$, Welch's $t$ test). (C) Representative Western blot showing α5-integrin and senescence/proliferation marker proteins (lamin-B1 and PCNA) in two independent yHDF lines derived from different young donors (yHDF$^1$ and yHDF$^2$) and aHDFs, with GAPDH as a loading control. (D) Quantification of Western blot results shown in C, presenting of α5-integrin, lamin-B1, and PCNA protein expression levels, normalized to GAPDH, and presented as relative values compared with yHDF$^1$. Bars represent the mean ± 95% confidence interval from four independent experiments. Statistical significance is indicated by **$p < 0.01$ and ***$p < 0.001$ (aHDF vs. yHDF$^{2:}$ $p = 1.55e{-}02$ for α5-integrin; aHDF vs. yHDF$^{2:}$ $p = 1.13e{-}04$ for lamin-B1; aHDF vs. yHDF$^{2:}$ $p = 7.36e{-}05$ for PCNA, Welch's $t$ test) (E) ITGA5 mRNA expression levels in yHDFs and aHDFs, measured by RNA-seq analysis (MATERIALS AND METHODS), presented as fragments per kilobase of transcript per million mapped reads.

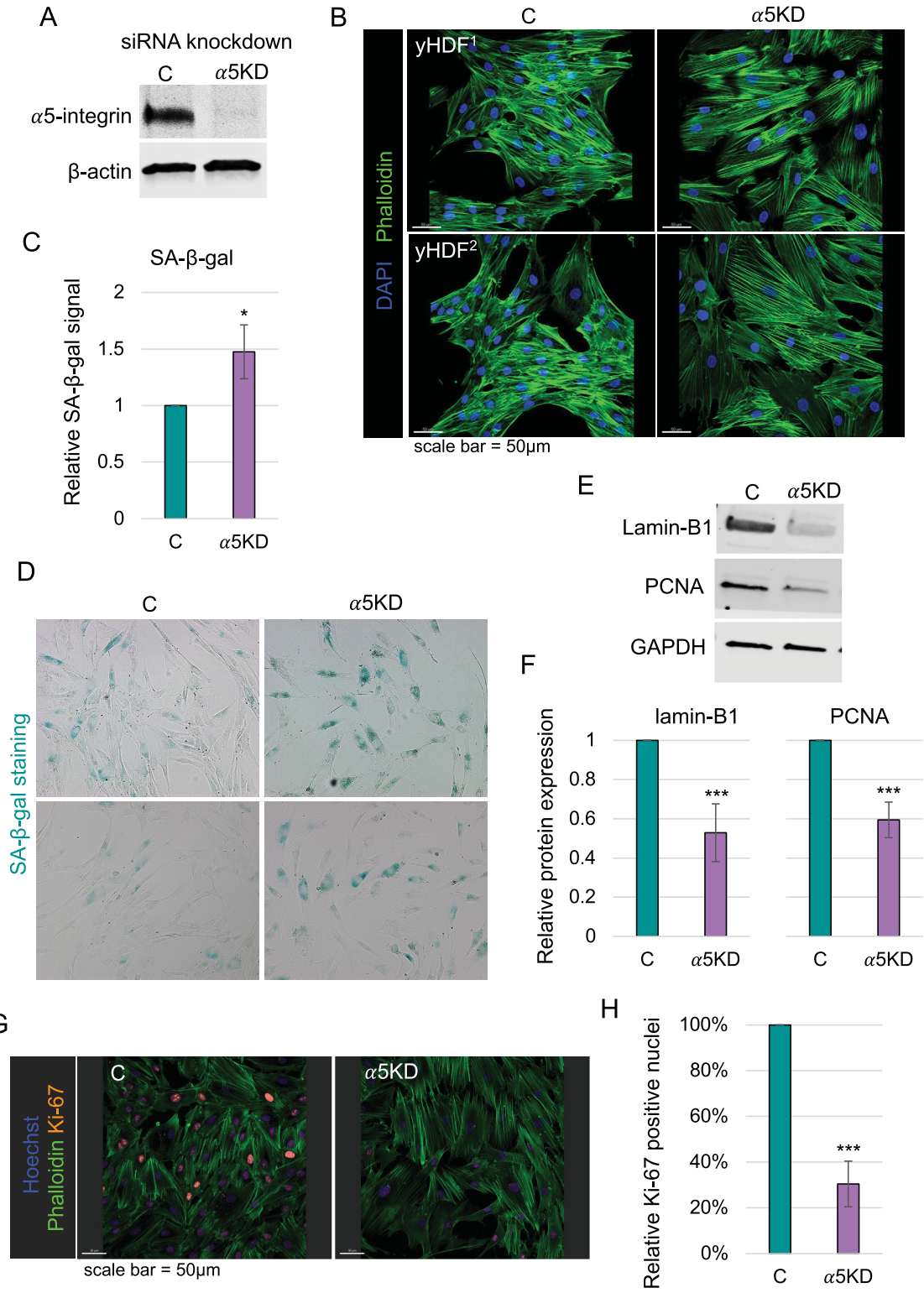


FIGURE 4: Loss of $\alpha$5-integrin leads to cellular senescence in yHDFs. (A) Western blot analysis showing the efficiency of $\alpha$5KD in yHDFs. The control (C) sample was transfected with negative control siRNAs. (B) Representative immunofluorescence images showing cellular morphology in $\alpha$5KD fibroblasts, with F-actin stained using phalloidin (green), and nuclei are stained with DAPI (blue). (C) Quantification of SA-$\beta$-gal staining in control (C) and $\alpha$5KD fibroblasts. Bars represent the mean $\pm$ 95% confidence interval from two independent experiments. Statistical significance is indicated by *$p < 0.05$ ($p = 2.97e{-}02$, Welch's $t$ test). (D) Representative SA-$\beta$-gal staining images of control (C) and $\alpha$5KD fibroblasts. (E) Representative Western blot showing senescence/proliferation marker proteins (lamin-B1 and PCNA) in control and $\alpha$5KD fibroblasts, with GAPDH as a loading control. (F) Quantification of Western blot results shown in D, presenting lamin-B1 and PCNA protein expression levels, normalized to GAPDH and presented

directly to cellular senescence, we cultured α5KD fibroblasts on cell-derived matrix (CDM) prepared from yHDFs. The CDM was generated by culturing yHDFs, followed by gentle cell dissociation to retain the ECM structure (MATERIALS AND METHODS). The structural integrity of the CDM was confirmed by FN and collagen-I staining (Supplemental Figure S6A).

Remarkably, when α5KD yHDFs were cultured on CDM, their proliferative capacity was significantly restored, reaching levels comparable with the control yHDFs. Proliferation was assessed by expression of PCNA and lamin-B1 (Figure 6, B and C), and Ki-67 (Figure 6, D and E). In contrast, coating with soluble FN alone failed to rescue proliferation in α5KD fibroblasts (Supplemental Figure S6B), suggesting that the fibrillar structure and composition of the CDM are essential for restoring proliferative potential. Consistent with these observations, culturing aHDFs on CDM also led to a marked increase in cell proliferation compared with FN-coated conditions, underscoring the ability of an intact ECMs in supporting fibroblast proliferation and partially rescuing the age-associated proliferative decline (Figure 6F).

## DISCUSSION

In this study, we provide insights into age-associated alterations in the FN ECM and the progression of cellular senescence in HDFs. Our findings reveal that aHDFs produce a significantly lower density of extracellular FN fibrils compared with yHDFs, which correlates with a reduction in α5-integrin expression on the cell surface. Notably, loss of α5-integrin alone is sufficient to induce cellular senescence, as demonstrated by elevated levels of senescence markers, decreased cell proliferation, and the enrichment of senescence-related gene sets in transcriptomic analyses. Interestingly, culturing α5-integrin–deficient cells on CDM significantly restores cell proliferation, suggesting that a rich ECM environment can compensate for α5-integrin loss. These results underscore the adaptability of cell–ECM interactions and the crucial role of ECM structure in maintaining cellular function and proliferative capacity.

A key question that remains to be answered is how α5-integrin is lost in aHDFs. Integrin levels are regulated by both transcriptional and posttranslational mechanisms (Kechagia *et al.*, 2019), but our data suggest that posttranscriptional regulation—likely involving protein turnover. Age-related changes in integrin production, degradation, or recycling may explain the observed reduction in α5-integrin levels in aHDFs. Specifically, the presence of integrins on the cell surface is dynamically controlled by intracellular trafficking processes, including endocytosis and exocytosis (Moreno-Layseca *et al.*, 2019; Kechagia *et al.*, 2019; Caswell *et al.*, 2009). Disruptions in these trafficking pathways during aging may impair α5-integrin recycling, leading to reduced surface expression and impaired FN ECM assembly.

Our findings suggest that a structured ECM environment, such as that provided by CDM, compensates for α5-integrin deficiency and restores cell proliferation. Future studies should examine whether specific ECM molecules, structural organization, physical properties of the ECM, or compensatory roles of other integrins support cell proliferation in α5KD cells. A deeper understanding of these ECM-based mechanisms could inform strategies to optimize ECM composition and organization to maintain fibroblast function in aging dermal tissue, potentially offering therapeutic approaches for age-related tissue dysfunction.

## MATERIALS AND METHODS

**Request a protocol through *Bio-protocol***

### Mouse skin section, staining, and dermal FN quantification

A total of six female C57BL/6J mice were used in this study, divided into two age groups: young mice ($n = 3$, ages 1.5–3 mo) and aged mice ($n = 3$, ages 17–21 mo). All animal procedures were conducted in accordance with the ethical guidelines approved by the Institutional Animal Care and Use Committee of the National University of Singapore. Mice were killed via $CO_2$ inhalation, and dorsal back skin was excised using sterile surgical instruments. The excised skin was washed with cold PBS to remove blood and debris, cut into small pieces, and fixed in 4% paraformaldehyde (PFA) at 4°C overnight. After fixation, tissues were embedded in optimal cutting temperature (OCT) compound and frozen in isopentane precooled with dry-ice. Frozen OCT blocks were stored on dry-ice for up to 1 h before transfer to −80°C until further use. Cryostat sections were cut at a thickness of 50 to 100 μm and immediately stored in PBS containing 0.2% sodium azide.

For immunostaining, free-floating tissue sections were permeabilized with 0.3% PBS-Triton X-100 and blocked for 1 to 2 h at room temperature (RT) in a solution containing 2.5% goat serum, 2% fish gelatin, and 1% BSA in 0.1% PBS-Triton X-100. Additional blocking was performed using the Mouse-on-Mouse kit (Vector Laboratories, #BMK-2202) for 1 h at RT. Primary antibody incubation was conducted overnight at 4°C using the anti-FN (1:200, Abcam, #ab2413). Following primary antibody incubation, sections were washed with 0.1% PBS-Triton X-100 and 0.1% PBS-Tween-20. Secondary antibody incubation was performed at RT for 2 h, followed by additional washes with 0.1% PBS-Triton X-100 and 0.1% PBS-Tween-20. To preserve tissue structure, sections were mounted using either a parafilm spacer or lanolin drops before placing the coverslips. Mounting medium with DAPI (Vector Laboratories, #H-1200-10) was applied for nuclear counterstaining and fluorescence preservation before sealing the coverslips. Immunostained tissue sections were imaged using confocal microscopy, and image processing and analysis were performed using Imaris Software (Oxford Instruments).

### HDFs culture

yHDF lines (GM09503: 10-y-old donor, GM01652: 11-y-old donor) and aHDF lines (GM01680: 71-y-old donor, GM01681: 70-y-old donor, and GM03525: 80-y-old donor) were obtained from the Coriell Institute for Medical Research (NJ). Fibroblast culture medium was prepared using minimum essential medium (MEM) (Life Technologies, #11095080), supplemented with 12.5% FBS (Life Technologies), and 1% MEM non-essential amino acids solution (Life Technologies, #11140050). Fibroblasts were maintained in a 37°C incubator with 5% $CO_2$. For 3D culture, HDFs were

as relative values compared with control. Bars represent the mean ± 95% confidence interval from six and nine independent experiments for lamin-B1 and PCNA, respectively. Statistical significance is indicated by ***$p < 0.001$ ($p = 1.51e{-}03$ for lamin-B1; $p = 3.47e{-}05$ for PCNA, Welch's *t* test). (G) Representative immunofluorescence images showing Ki-67 (orange) as a marker for cell proliferation, phalloidin (green) to stain F-actin filaments, and Hoechst (blue) to stain nuclei in control and α5KD cells. (H) Quantification of Ki-67–positive nuclei, expressed relative to the control (C), in control and α5KD fibroblasts. Bars represent mean ± 95% confidence interval from seven independent experiments. Statistical significance is indicated by ***$p < 0.001$ ($p = 9.36e{-}06$, Welch's *t* test).

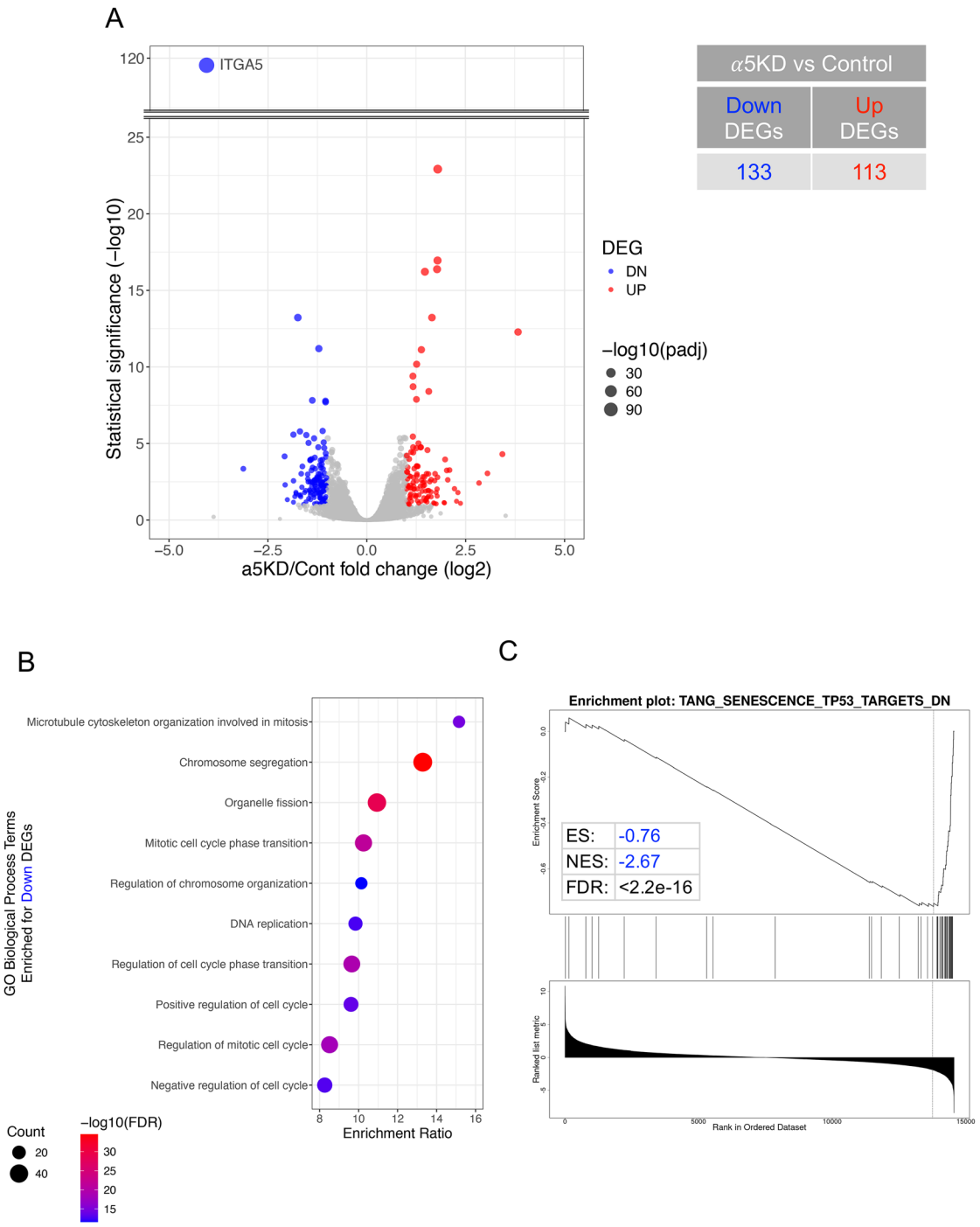


FIGURE 5: Transcriptomic changes following $\alpha$5KD in yHDFs. (A) Volcano plot of differential gene expression. The plot shows the $\log_2$ fold change in gene expression ($\alpha$5KD vs. control) on the *x*-axis and the statistical significance ($-\log_{10}$ adjusted *p* value) on the *y*-axis. Significantly, downregulated genes are highlighted in blue, while upregulated genes are shown in red. ITGA5 is among the most downregulated genes. The total number of DEGs is indicated in the box on the right, with 133 downregulated and 113 upregulated genes. (B) GO biological process terms enriched for downregulated DEGs. The dot plot displays the enrichment ratio (*x*-axis) for significantly enriched GO terms among downregulated DEGs in $\alpha$5KD fibroblasts. Each dot represents a GO term, with dot size indicating the number of associated genes and color representing the $-\log_{10}$ false discovery rate. (C) The GSEA enrichment plot illustrating the distribution of gene ranked by their differential expression ($\alpha$5KD vs. control HDFs) along the horizontal axis. Vertical bars indicate the position of genes from the senescence-related gene set within this ranked list. The enrichment score (ES) curve reaches a peak negative score of −0.76, with a normalized ES of −2.67, indicating the maximal enrichment of this gene set in the downregulated portion of the ranked list. The GSEA is based on previously established senescence-related gene sets, as described in Tang *et al.* (2007).

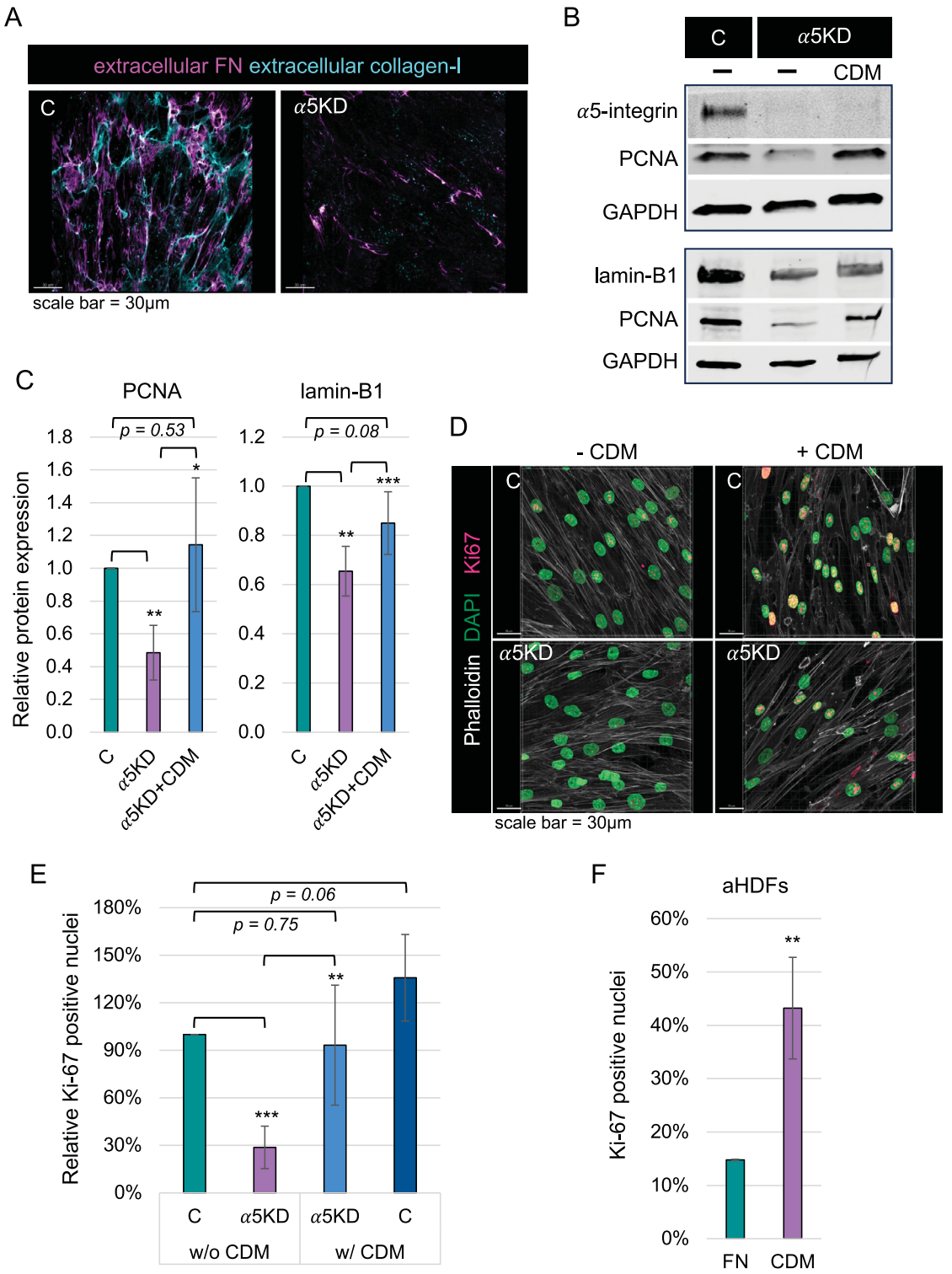


FIGURE 6: CDM significantly rescues cell proliferation defects in α5KD and aged HDFs. (A) Representative immunofluorescence images showing extracellular FN (magenta) and collagen-I (cyan)) in control (C) and α5KD fibroblasts. (B) Representative Western blot showing α5-integrin, PCNA, and lamin-B1 expression in control (C) and α5KD fibroblasts cultured under different substrate conditions: without CDM (−) and with CDM. The top and bottom panels were obtained from separate gels, as indicated by the boxed groupings. GAPDH is shown as a loading control for each gel. (C) Quantification of Western blot results shown in B, presenting α5-integrin, PCNA, and lamin-B1 protein expression in control (C) and α5KD fibroblasts cultured with and without CDM. Protein levels are normalized to GAPDH and presented as values relative to the control sample. Bars represent the mean ± 95% confidence interval from five independent experiments. Statistical significance is indicated by ***$p < 0.001$, **$p < 0.01$, and *$p < 0.05$ ($p = 2.57e{-}02$ for PCNA in α5KD vs. α5KD+CDM; $p = 8.84e{-}03$ for lamin-B1 level α5KD vs. α5KD+CDM, paired *t* test).

embedded in collagen-I gels prepared according to the protocol provided by ibidi (ibidi, 2023), using Collagen I, rat tail (Life Technologies, #A1048301) at a final concentration of 1.25 mg/ml.

### Fluorescence immunostaining and confocal microscopy

For fluorescence immunostaining, samples were fixed with 4% PFA for 15 min at RT, followed by two rinses with PBS. For intracellular protein staining, samples were permeabilized with 0.2% PBS-Triton X-100 for 15 min. In contrast, for ECM protein staining, no permeabilization was performed, and detergents were omitted from all subsequent washing steps. Samples were then incubated with the primary antibody overnight at 4°C, followed by three washes with 0.1% PBS-Triton X-100 for 5 min each. The secondary antibody was applied either overnight at 4°C or for 1 h at RT, followed by three additional washes in 0.1% PBS-Triton X-100. For nuclear and cytoskeletal staining, samples were counterstained with DAPI or Hoechst and Phalloidin, then imaged using confocal microscopy on either the Nikon A1Rsi or Zeiss LSM980 systems. Image analysis was performed using Imaris (Oxford Instruments) or FIJI (ImageJ, (Schindelin *et al.*, 2012).

The following antibodies used:

- FN1 antibody (1:200, Abcam, #ab2413).
- SNAKA51 antibody (1:400, Millipore, #MABT201).
- Collagen-I antibody (1:200, Cell Signaling Technology, #66948).
- Ki-67 antibody (1:1000, Cell Signaling Technology, #9129).

### SA-$\beta$-gal staining

Cells were fixed with a solution containing 2% formaldehyde and 2% glutaraldehyde at RT for 15 min. The $\beta$-gal staining reagent was prepared in water with the following components:

- 1 mg/ml X-gal dissolved in dimethylformamide.
- 40 mM citric acid/sodium phosphate buffer (pH 6.0).
- 5 mM potassium ferrocyanide.
- 5 mM potassium ferricyanide.
- 150 mM sodium chloride.
- 2 mM magnesium chloride.

One ml of the $\beta$-gal reagent was added to each glass-bottom dish (IWAKI, 27 mm in diameter). The sample dishes were then sealed, covered with aluminum foil, and incubated at 37°C overnight. Imaging of SA-$\beta$-gal–stained samples was performed using a Nikon Ti-E microscope, and image analysis was conducted using FIJI (ImageJ; Schindelin *et al.*, 2012).

### siRNA transfection, RNA-seq, and analysis

siRNA transfections were performed using Lipofectamine RNAiMAX (Invitrogen, # 13778030) according to the manufacturer's instructions. siRNAs targeting ITGA5 (hs.Ri.ITGA5.13.1-3) and a negative control siRNA (#51-01-14-03) were obtained from Integrated DNA Technologies. Cells were transfected for 2 d, then trypsinized and replated into new culture vessels under different substrate conditions depending on the experimental setup: uncoated, coated with 0.2% gelatin (Sigma, #G1393), or 10 µg/ml FN (Roche, #10838039001). For RNA-seq experiments, cells were similarly transfected for 2 d, then trypsinized and replated into uncoated culture vessels for an additional 2 d. Total RNA was extracted using the RNeasy Plus Micro Kit (QIAGEN, #74034) with three replicates per condition. RNA library preparation and sequencing were outsourced to BGI Genomics (Hong Kong). Initial data processing, including quality control, alignment, and quantification, was performed with their Dr. Tom analysis system (BGI Genomics). Read count data were analyzed using the DESeq2 (Love *et al.*, 2014). DEGs were identified based on a threshold of $|\log_2$ fold change$| > 1$ and adjusted $p$ value of $<0.1$. Overrepresentation analysis of GO terms and GSEA were conducted using WebGestalt (Elizarraras *et al.*, 2024), based on statistical outputs from DESeq2. Visualizations of enrichment results were generated using ggplot2 (Wickham, 2016).

### Western blot

Samples for Western blot analysis were washed twice with ice-cold PBS, then lysed by scraping with Laemmli protein sample buffer (Bio-Rad, #1610737) supplemented with 50 mM DTT on ice. Lysates were subsequently frozen at −80°C. Upon thawing on ice, samples were boiled at 95°C for 5 min, followed by centrifugation at 13,000 rpm for 10 min. The supernatant was then loaded onto a Mini-PROTEAN TGX Precast Gel (4–10%) (Bio-Rad) for SDS–PAGE, which was run at 200 V for 30 min. Proteins were transferred onto a nitrocellulose membrane using the Trans-Blot Turbo transfer system (Bio-Rad). Membranes were blocked at RT for 1 h using Intercept PBS-blocking buffer (Li-Cor) diluted 1:1 in 0.2% PBS-Tween 20. The membrane was incubated with the primary antibody overnight at 4°C, followed by three washes (5 min each) with 0.2% PBS-Tween 20. Next, the secondary antibodies (Li-Cor) were applied at RT for 1 h, followed by three additional washes (5 min each) with 0.2% PBS-Tween 20. A final wash with PBS was performed before imaging with the Odyssey DLx imaging system (Li-Cor) for protein band visualization. Protein band quantification was conducted using FIJI (ImageJ; Schindelin *et al.*, 2012). The following antibodies used:

- Integrin $\alpha$5 antibody (1:2000, Abcam, #ab150361).
- Lamin-B1 antibody (1:5000, Abcam, #ab16048).
- PCNA antibody (1:2000, Cell Signaling Technology, #2586).
- GAPDH antibody (1:5000, Cell Signaling Technology, #5174).

### CDM preparation

CDM was prepared following the method described by Kaukonen *et al.* (2017). In brief, young fibroblasts were seeded at subconfluent levels on gelatin-coated dishes and cultured for at least 6 d to allow for ECM generation. Fibroblasts were then removed using a mild decellularization solution containing 2% $NH_4OH$ and 0.5% Triton X-100 in PBS, followed by three thorough washes with

(D) Representative immunofluorescence images of Ki-67 expression in control and $\alpha$5KD fibroblasts, cultured with or without CDM. Ki-67 (pink) is used as a marker for cell proliferation, phalloidin (gray) stains actin filaments, and DAPI (green) stains nuclei. (E) Quantification of the Ki-67–positive nuclei, expressed relative to the control sample (C without CDM), in control (C) and $\alpha$5KD fibroblasts cultured with or without CDM. Bars represent mean ± 95% confidence interval from five independent experiments. Statistical significance is indicated by *** $p < 0.001$ and ** $p < 0.01$ ($p = 4.70e{-}04$ for C vs. $\alpha$5KD without CDM, Welch's $t$ test; $p = 1.39e{-}02$ for $\alpha$5KD without CDM vs. $\alpha$5KD with CDM, paired $t$ test). (F) Quantification of the Ki-67–positive nuclei in aHDFs cultured in without CDM (FN-coated, FN) or with CDM. Bars represent the mean ± 95% confidence interval from six independent experiments. Statistical significance is indicated by ** $p < 0.01$ ($p = 2.06e{-}03$, Welch's $t$ test).

PBS. The resulting CDM was stored in DPBS supplemented with 1% penicillin–streptomycin at 4°C for subsequent experiments.


## ACKNOWLEDGMENTS

We would like to thank Jennifer Young (MBI, NUS) for her insightful discussions and constructive feedback, Hui Ting Ong (MBI, NUS) for her assistance with microscopy image analysis, and Jinrong Hu for sharing reagents and the protocol for SA-$\beta$-gal staining. This work was supported by grant A-0007081-00-00 from the National University of Singapore and grant NRF-MSG-2023-0001 from Singapore National Research Foundation to R.L., and by a grant from the National University of Singapore Bia-Echo Asia Center for Reproductive Longevity and Equality (ACRLE).


## REFERENCES


Caswell PT, Vadrevu S, Norman JC. (2009). Integrins: Masters and slaves of endocytic transport. Nat Rev Mol Cell Biol 10, 843–853.

Chin T, Lee XE, Ng PY, Lee Y, Dreesen O. (2023). The role of cellular senescence in skin aging and age-related skin pathologies. Front Physiol 14, 1297637.

Cho KA, Ryu SJ, Oh YS, Park JH, Lee JW, Kim HP, Kim KT, Jang IS, Park SC. (2004). Morphological adjustment of senescent cells by modulating caveolin-1 status. J Biol Chem 279, 42270–42278.

Cole MA, Quan T, Voorhees JJ, Fisher GJ. (2018). Extracellular matrix regulation of fibroblast function: Redefining our perspective on skin aging. J Cell Commun Signal 12, 35–43.

Database, Reactome Pathway. (2024). Reactome_cellular_senescence. Available at: https://www.reactome.org/content/detail/R-HSA-2559583.

Dreesen O, Chojnowski A, Ong PF, Zhao TY, Common JE, Lunny D, Lane EB, Lee SJ, Vardy LA, Stewart CL, Colman A. (2013). Lamin B1 fluctuations have differential effects on cellular proliferation and senescence. J Cell Biol 200, 605–617.

Elizarraras JM, Liao Y, Shi Z, Zhu Q, Pico AR, Zhang B. (2024). WebGestalt 2024: Faster gene set analysis and new support for metabolomics and multi-omics. Nucleic Acids Res 52, W415–W421.

Fane M, Weeraratna AT. (2020). How the ageing microenvironment influences tumour progression. Nat Rev Cancer 20, 89–106.

Fisher GJ, Quan T, Purohit T, Shao Y, Cho MK, He T, Varani J, Kang S, Voorhees JJ. (2009). Collagen fragmentation promotes oxidative stress and elevates matrix metalloproteinase-1 in fibroblasts in aged human skin. Am J Pathol 174, 101–114.

Fleischer JG, Schulte R, Tsai HH, Tyagi S, Ibarra A, Shokhirev MN, Huang L, Hetzer MW, Navlakha S. (2018). Predicting age from the transcriptome of human dermal fibroblasts. Genome Biol 19, 221.

Fligiel SE, Varani J, Datta SC, Kang S, Fisher GJ, Voorhees JJ. (2003). Collagen degradation in aged/photodamaged skin in vivo and after exposure to matrix metalloproteinase-1 in vitro. J Invest Dermatol 120, 842–848.

Freund A, Laberge RM, Demaria M, Campisi J. (2012). Lamin B1 loss is a senescence-associated biomarker. Mol Biol Cell 23, 2066–2075.

Fridman AL, Tainsky MA. (2008). Critical pathways in cellular senescence and immortalization revealed by gene expression profiling. Oncogene 27, 5975–5987.

Giancotti FG, Ruoslahti E. (1999). Integrin signaling. Science 285, 1028–1032.

Graham J, Raghunath M, Vogel V. (2019). Fibrillar fibronectin plays a key role as nucleator of collagen I polymerization during macromolecular crowding-enhanced matrix assembly. Biomater Sci 7, 4519–4535.

Haydont V, Bernard BA, Fortunel NO. (2019). Age-related evolutions of the dermis: Clinical signs, fibroblast and extracellular matrix dynamics. Mech Ageing Dev 177, 150–156.

Hynes RO (2002). Integrins: Bidirectional, allosteric signaling machines. Cell 110, 673–687.

ibidi. (2023). Application Note 26: Preparation of collagen I gels. Available at: https://ibidi.com/img/cms/support/AN/AN26_CollagenI_protocols.pdf.

Kaukonen R, Jacquemet G, Hamidi H, Ivaska J. (2017). Cell-derived matrices for studying cell proliferation and directional migration in a complex 3D microenvironment. Nat Protoc 12, 2376–2390.

Kechagia JZ, Ivaska J, Roca-Cusachs P. (2019). Integrins as biomechanical sensors of the microenvironment. Nat Rev Mol Cell Biol 20, 457–473.

Love MI, Huber W, Anders S. (2014). Moderated estimation of fold change and dispersion for RNA-seq data with DESeq2. Genome Biol 15, 550.

McCabe MC, Hill RC, Calderone K, Cui Y, Yan Y, Quan T, Fisher GJ, Hansen KC. (2020). Alterations in extracellular matrix composition during aging and photoaging of the skin. Matrix Biol Plus 8, 100041.

McDonald JA, Kelley DG, Broekelmann TJ. (1982). Role of fibronectin in collagen deposition: Fab' to the gelatin-binding domain of fibronectin inhibits both fibronectin and collagen organization in fibroblast extracellular matrix. J Cell Biol 92, 485–492.

Moreno-Layseca P, Icha J, Hamidi H, Ivaska J. (2019). Integrin trafficking in cells and tissues. Nat Cell Biol 21, 122–132.

Moreno-Layseca P, Streuli CH. (2014). Signalling pathways linking integrins with cell-cycle progression. Matrix Biol 34, 144–153.

Panwar P, Butler GS, Jamroz A, Azizi P, Overall CM, Bromme D. (2018). Aging-associated modifications of collagen affect its degradation by matrix metalloproteinases. Matrix Biol 65, 30–44.

Plikus MV, Wang X, Sinha S, Forte E, Thompson SM, Herzog EL, Driskell RR, Rosenthal N, Biernaskie J, Horsley V. (2021). Fibroblasts: Origins, definitions, and functions in health and disease. Cell 184, 3852–3872.

Saul D, Kosinsky RL, Atkinson EJ, Doolittle ML, Zhang X, LeBrasseur NK, Pignolo RJ, Robbins PD, Niedernhofer LJ, Ikeno Y, *et al.* (2022). A new gene set identifies senescent cells and predicts senescence-associated pathways across tissues. Nat Commun 13, 4827.

Schindelin J, Arganda-Carreras I, Frise E, Kaynig V, Longair M, Pietzsch T, Preibisch S, Rueden C, Saalfeld S, Schmid B, *et al.* (2012). Fiji: An open-source platform for biological-image analysis. Nat Methods 9, 676–682.

Schwarzbauer JE, DeSimone DW. (2011). Fibronectins, their fibrillogenesis, and in vivo functions. Cold Spring Harb Perspect Biol 3, a005041.

Shimi T, Butin-Israeli V, Adam SA, Hamanaka RB, Goldman AE, Lucas CA, Shumaker DK, Kosak ST, Chandel NS, Goldman RD. (2011). The role of nuclear lamin B1 in cell proliferation and senescence. Genes Dev 25, 2579–2593.

Singh P, Carraher C, Schwarzbauer JE. (2010). Assembly of fibronectin extracellular matrix. Annu Rev Cell Dev Biol 26, 397–419.

Sole-Boldo L, Raddatz G, Schutz S, Mallm JP, Rippe K, Lonsdorf AS, Rodriguez-Paredes M, Lyko F. (2020). Single-cell transcriptomes of the human skin reveal age-related loss of fibroblast priming. Commun Biol 3, 188.

Sottile J, Shi F, Rublyevska I, Chiang HY, Lust J, Chandler J. (2007). Fibronectin-dependent collagen I deposition modulates the cell response to fibronectin. Am J Physiol Cell Physiol 293, C1934–C1946.

Subramanian A, Tamayo P, Mootha VK, Mukherjee S, Ebert BL, Gillette MA, Paulovich A, Pomeroy SL, Golub TR, Lander ES, Mesirov JP. (2005). Gene set enrichment analysis: A knowledge-based approach for interpreting genome-wide expression profiles. Proc Natl Acad Sci USA 102, 15545–15550.

Tang X, Milyavsky M, Goldfinger N, Rotter V. (2007). Amyloid-beta precursor-like protein APLP1 is a novel p53 transcriptional target gene that augments neuroblastoma cell death upon genotoxic stress. Oncogene 26, 7302–7312.

Varani J, Dame MK, Rittie L, Fligiel SE, Kang S, Fisher GJ, Voorhees JJ. (2006). Decreased collagen production in chronologically aged skin: Roles of age-dependent alteration in fibroblast function and defective mechanical stimulation. Am J Pathol 168, 1861–1868.

Wickham H (2016). ggplot2: Elegant Graphics for Data Analysis. Use R!, 1 online resource (XVI, 260 pages 32 illustrations, 140 illustrations in color. Cham: Springer International Publishing: Imprint: Springer.